

# Sphere Extraction in MR Images with Application to Whole-Body MRI

Christian Wachinger<sup>a</sup>, Simon Baumann<sup>a</sup>, Jochen Zeltner<sup>b</sup>, Ben Glocker<sup>a</sup>, and Nassir Navab<sup>a</sup>

<sup>a</sup>Computer Aided Medical Procedures (CAMP), Technische Universität München, Germany.

<sup>b</sup>Siemens Medical Solutions, Erlangen, Germany

## ABSTRACT

Recent technological advances in magnetic resonance imaging (MRI) lead to shorter acquisition times and consequently make it an interesting whole-body imaging modality. The acquisition time can further be reduced by acquiring images with a large field-of-view (FOV), making less scan stations necessary. Images with a large FOV are however disrupted by severe geometric distortion artifacts, which become more pronounced closer to the boundaries. Also the current trend in MRI, towards shorter and wider bore magnets, makes the images more prone to geometric distortion.

In a previous work,<sup>4</sup> we proposed a method to correct for those artifacts using simultaneous deformable registration. In the future, we would like to integrate previous knowledge about the distortion field into the process. For this purpose we scan a specifically designed phantom consisting of small spheres arranged in a cube. In this article, we focus on the automatic extraction of the centers of the spheres, wherein we are particularly interested, for the calculation of the distortion field.

The extraction is not trivial because of the significant intensity inhomogeneity within the images. We propose to use the local phase for the extraction purposes. The phase has the advantage that it provides structural information invariant to intensity. We use the monogenic signal to calculate the phase. Subsequently, we once apply a Hough transform and once a direct maxima search, to detect the centers. Moreover, we use a gradient and variance based approach for the radius estimation. We performed our extraction on several phantom scans and obtained good results.

**Keywords:** Segmentation, Pattern Recognition

## 1. INTRODUCTION

Technological developments in magnetic resonance imaging, such as multi-channel receiver, parallel imaging techniques, and automated table movement, made it a popular whole-body imaging modality challenging the standard modality CT.<sup>1</sup>

MRI has several advantages in comparison to CT: the better soft-tissue contrast, no radiation, non-iodine based contrast agents, better detection of lesions, and is better suited for screening purposes. First clinical studies show its value in oncological applications, which focus on the search for metastases of cancer patients in the whole-body. Lauenstein *et al.*<sup>2</sup> found out that it compares well with the standard methods (CT, PET and nuclear scintigraphy) for the detection of cerebral, pulmonary, and hepatic lesions and is more sensitive for detection of hepatic and osseous metastases. Additionally, the excellent contrast of MRI provides further information about soft tissue and organs to the physician, supporting his diagnosis.<sup>3</sup>

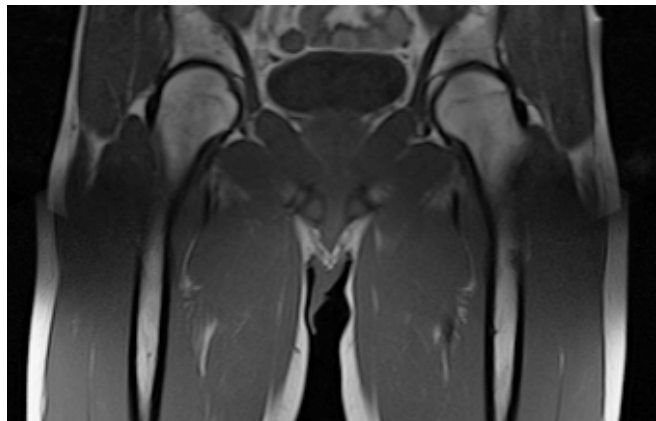


Figure 1. Overlay of two consecutive MR scans with a significant geometric distortion, visible in the middle of the image.

The major drawback, next to the higher costs and less trained personnel available, is the longish scanning time for a whole-body scan with MRI. We are interested in reducing the scanning time by acquiring images with a large field-of-view (FOV), enabling to cover with the same number of scans larger parts of the body. This, however, has the negative effect that

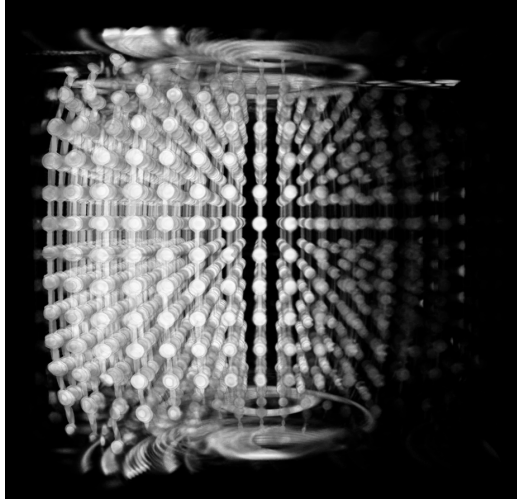


Figure 2. Volume Rendering of the Phantom.

geometric distortion artifacts that are negligible close to the magnetic iso-center become visible towards the boundaries of the images. Stitching together those images leads to discontinuities in the final image. An overlay of two consecutive MR scans is shown in Figure 1, where the significant distortion becomes apparent in the middle of the image. But geometric distortion is not only a problem for whole-body imaging, it is also problematic for other applications like radiation therapy treatment planning, where a high geometric accuracy is needed for navigation.

Geometric distortion can be split up into two groups, *system specific* and *object specific* distortions. System specific distortions occur due to inhomogeneities of the static magnetic field  $B_0$ , non-linearities of the gradient field, and eddy currents during gradient switch. In contrast, object or patient specific distortions, arise from susceptibility effects, chemical shift, and flow.<sup>5</sup> Essential for the spatial encoding in MRI is the Larmor equation, which relates the precession frequency of nuclear spins  $\omega$  to the magnetic field  $B$  using the gyromagnetic ratio  $\gamma$

$$\omega(x) = \gamma B(x) = \gamma(B_0 + x \cdot G_x) \quad (1)$$

with  $G_x$  the gradient field in  $x$  direction. It becomes apparent that non-uniformity of  $B_0$  and non-linearity of  $G_x$  will lead to geometric distortions in the reconstructed image.<sup>5</sup>

In the literature, mainly system-specific artifacts are discussed. Chang and Fitzpatrick<sup>6</sup> correct for  $B_0$  distortion by acquiring two almost identical images only differing in the polarity of the read-out gradient. This enables for an exact correction of  $B_0$  distortion. In follow-up articles Kannengiesser *et al.*<sup>7</sup> and Reinsberg *et al.*<sup>8</sup> refine this method by using deformable image registration techniques to make it also applicable to real MR images and not only phantom scans. This approach is hardly applicable in the clinical workflow because acquisition time would double. Doran *et al.*<sup>9</sup> analyze the distortion with phantom scans and apply the deduced correction field to medical data. It is doubtful if corrections based on phantom scans *alone* make sense because it is not feasible to build a phantom duplicating a biological system.<sup>6</sup>

In a recent work,<sup>4</sup> we proposed a new method for the correction of geometric distortion in whole-body imaging by applying a simultaneous non-rigid registration. The correction is not trivial because we do not have a target image that we can the image warp to. This is a similar to the problem that people in atlas construction are facing. We therefore adapted one of their approaches. We are iteratively registering overlapping images to the average image. The advantage of our approach is that we correct for both types of geometric distortions. A drawback is that we do not take any system specific information into consideration. Like Doran *et al.*,<sup>9</sup> we will try to measure the system specific distortion field (SSDF) with a specifically designed phantom. Our approach will however not only consider the application of the SSDF to the data, but instead either use it as a pre-processing step of the registration, or directly integrate it as prior knowledge into the registration process. We expect that the result of the registration will get better because we will already have corrected for a part of the distortion before the actual registration starts, giving the optimizer a starting point closer to the expected optimum.

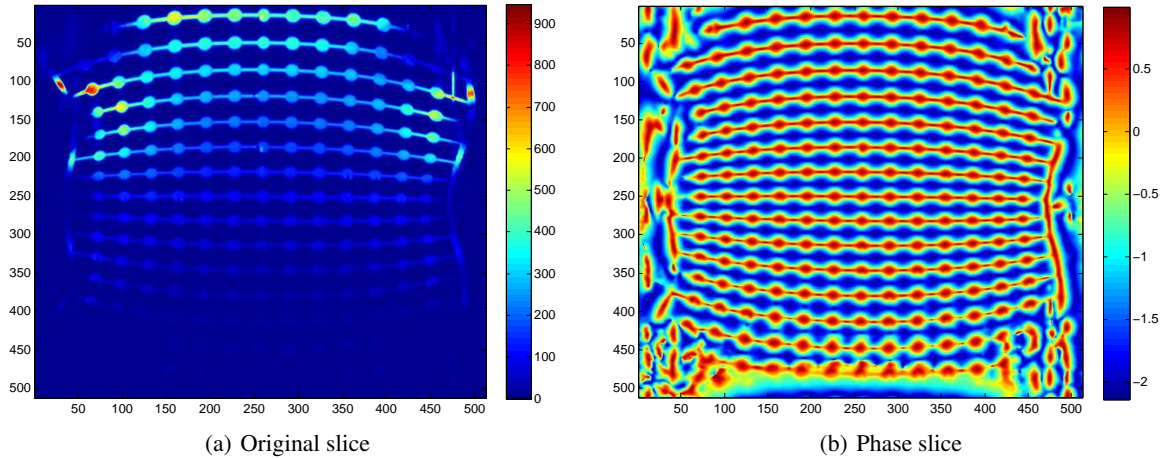


Figure 3. The original slice of the phantom shows a high intensity inhomogeneity. The phase image is able to capture the structural information, independent of the intensity.

In order to be able to estimate the SSDF, we measure the distortion in a specifically designed MR phantom consisting of small, water-filled spheres arranged in a cube, see Figure 2. The idea is to model the distortion field by comparing the physically exact center locations to the center locations detected in the MR images. During our experiments we found out that the automatic extraction of the spheres is a non-trivial task. The main reason is the significant intensity inhomogeneity within the images. To the best of our knowledge, the extraction of spheres in MR images has not yet been addressed. We propose an algorithm for this task based on the calculation of the local phase.

## 2. METHOD

Before describing the method in detail, we would like to briefly summarize the problem. Given is a scan of the spheres phantom in which we want to automatically determine the center of the spheres and also their radius to evaluate the result. Beforehand, we know neither the radius of the spheres, nor their distances from each other. We know, however, that the phantom is completely regular, so that we can measure the distances of the spheres close to the iso-center and extrapolate from this to obtain a model of the whole phantom. A volume rendering of a phantom scan is shown in Figure 2 and a single slice in Figure 3(a).

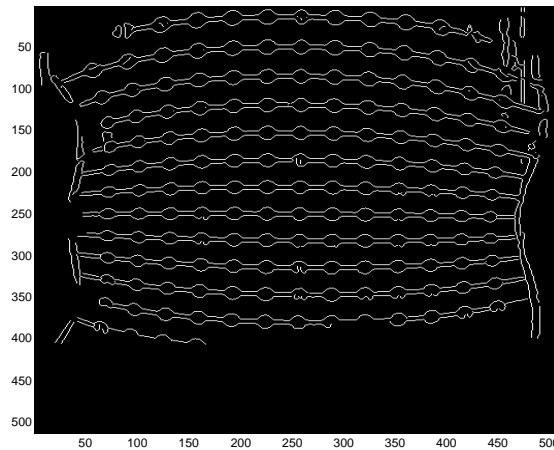


Figure 4. Output of Canny edge detector of the slice shown in 3(a).

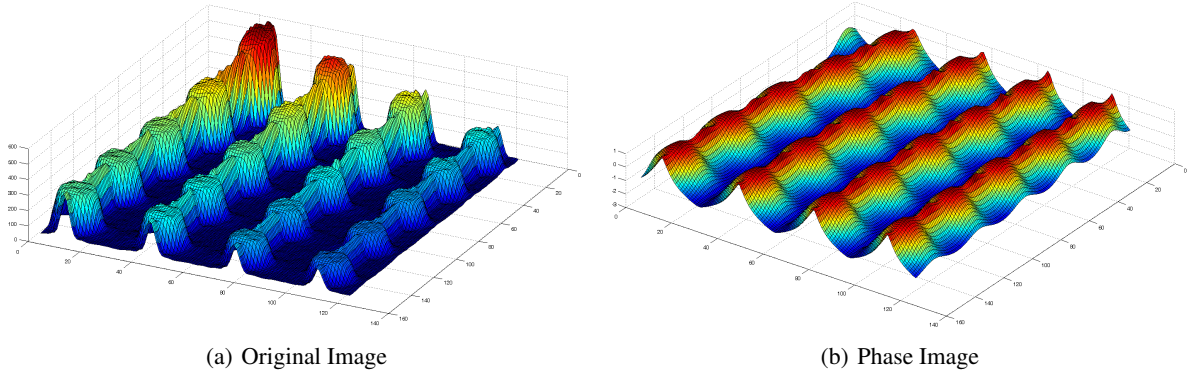


Figure 5. Plot of intensity values of original slice and phase slice. The region shown is a cut-out of Figure 3(a).

## 2.1 Hough Transform

One of the standard methods to calculate the center of a sphere is to apply a Hough transform.<sup>10</sup> We use the Hough transform with a fixed radius because all spheres we are searching for have the same radius and this enables us to reduce the complexity. Before applying the Hough transform, an edge detection has to be performed to extract the surface of the sphere. Due to the significant intensity inhomogeneity in the images, see Figures 2 and 3(a), the result obtained with a standard edge detection method such as Canny edge detector, is not satisfying, see Figure 4. Obviously, starting from such an image, the Hough transform cannot detect all the spheres.

## 2.2 Phase-Based Feature Detection

The method we are proposing calculates the local phase from image. Local properties of a 1D real signal  $f(x)$  are defined with the analytic signal  $f_A(x)$

$$f_A(x) = f(x) + i \cdot f_{\mathcal{H}}(x) \quad (2)$$

with  $i = \sqrt{-1}$  and  $f_{\mathcal{H}}(x)$  the Hilbert transform of  $f(x)$ . The local amplitude  $A(x)$  and local phase  $\phi(x)$  are:

$$A(x) = \sqrt{f^2(x) + f_{\mathcal{H}}^2(x)} \quad (3)$$

$$\phi(x) = \arctan(f(x)/f_{\mathcal{H}}(x)). \quad (4)$$

The local phase provides us with structural information, invariant to brightness and contrast. Taking a look at the images in Figure 3(a), these are the properties we are looking for in the sphere extraction. The analytic signal only works for 1D signals, but we have to handle 3D data. There are different approaches to extend this concept to  $N$ -D. Here we will use the *monogenic signal*.<sup>11</sup> It uses a generalization of the Hilbert transform, the Riesz transform, to calculate phase information in  $N$ -D. The image is filtered by  $N$  filters, which are given in the Fourier domain by

$$R_i(g_1, \dots, g_N) = \frac{g_i}{\sqrt{\sum_{j=1}^N g_j^2}} \quad (5)$$

with  $g_1, \dots, g_N$  the Fourier domain coordinates. We follow<sup>12,13</sup> in applying log-Gabor filters prior to the calculation of the monogenic signal of the image to extract frequency and spatial localization.

The phase image corresponding to the original slice Figure 3(a), is shown in Figure 3(b). One can clearly see that we get structural information all over the image, even though there is a significant intensity variation in the image. This is further illustrated in Figure 5, where we show a surface plot of the intensity of the slice. One clearly sees the intensity variation inside the original image, and the uniform output of the phase image.

## 2.3 Sphere Extraction

Continuing with the phase image, we have to extract the spheres in them. We present two different ways to proceed, where both led to good results.

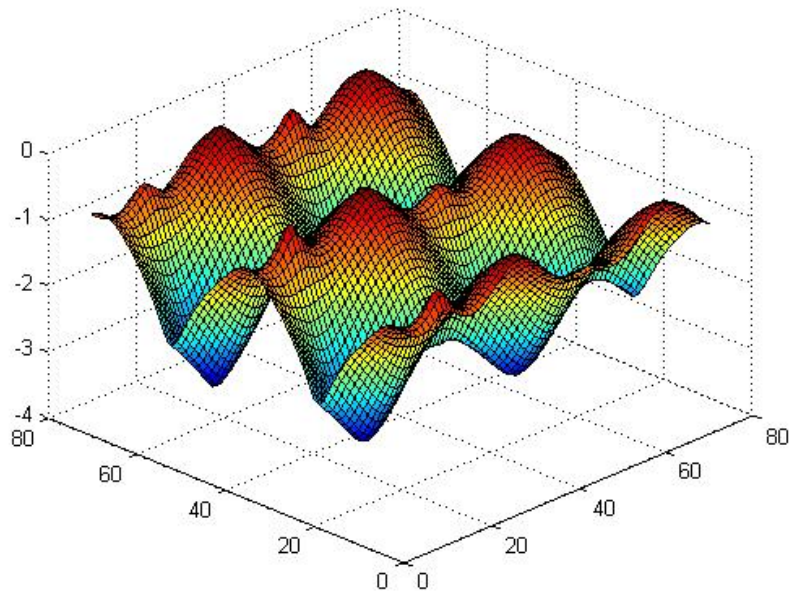


Figure 6. Surface plot of intensity values in local phase image. The tube, connecting the spheres, leads to side-maxima.

### 2.3.1 Hough Transform

The first approach is to run an edge detector on the phase image and subsequently apply the Hough transform. Here, it has to be taken into consideration that MR images are frequently acquired with an anisotropic voxel spacing, which has to be considered in the accumulator space.

### 2.3.2 Direct Maxima Search

The second approach after looking at the intensity surface of one slice, see Figure 5, is the direct search for the local maxima. In the original images, we have plateaus indicating the spheres. In the phase image, we see, in contrast, a smooth surface with local maxima at the respective sphere centers. Unfortunately, we can only show slices and cannot directly visualize the 3D phase volume, but the behavior is analogously.

As can also be seen in the images, the spheres are connected by tubes. These were necessary for distributing the water in the phantom. These tubes lead to side-maxima, which have to be discarded, see Figure 6. We eliminated the side-maxima by checking for rotational symmetry around the possible center. One can imagine this as laying a small sphere around the detected maximum and checking whether all the points on the sphere have about the same intensity values.

## 2.4 Radius Estimation

The estimation of the radius is not needed to calculate the distortion field, it just relies on the centers, but it is useful to evaluate the result. We use two different approaches. The first is to estimate the radius by calculating the y-gradient (perpendicular to tubes), identify the inflection point, and gauge its distance to the center. An example gradient image and measured radii are shown in Figure 7. The second approach is to put a cube, a bit larger than the maximal sphere radius around it. We then try out different radii, and calculate the variance of the intensity within the sphere and the variance of the intensity outside the sphere but inside the cube. Adding these two values gives us a cost function indicating the best radius.

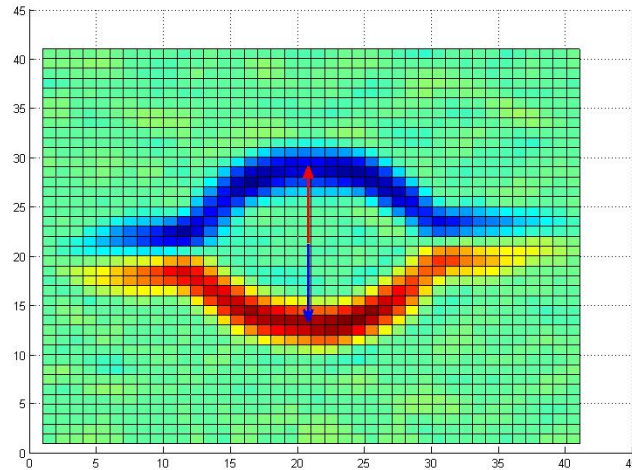


Figure 7. Radius estimation on gradient image of the phase image.

### 3. RESULTS

During our experiments we have not found any major difference between the two approaches for the center extraction. In Figure 9, we show the result of the extraction using the local maxima search. Centers are indicated with white dots, in case they are lying in this slice. In Figures 8(a) and 8(b), a histogram of the detected radii is shown for the method using the deflection point and the variance calculation, respectively. One can see that both times a radius of 8 is most likely, where we have a certain variation due to the geometric distortion.

### 4. CONCLUSION

We addressed the subject of calculating deformation fields by acquiring phantom data of a specifically designed spheres phantom. The extraction of spheres is difficult due to intensity inhomogeneities, so that we applied the sphere detection on the local phase image. The direct application of the Hough transform was not possible because of the low quality of the edge image. The local phase image provides structural information independent of brightness and contrast. We investigated the usage of the Hough transform on the phase image and also the direct estimation of local maxima for finding the sphere centers. Both approaches lead to good results, where for the local maxima estimation special care has to be taken of side-maxima. Moreover, we presented two approaches for the estimation of the radius of the spheres. The first one measures the distance of the center to the deflection point identified on the gradient image of the phase image. The second one poses the radius estimation as an optimization problem, with the variance as cost function. The results we obtained are very promising and we will continue evaluating our method on further phantom scans.

**Acknowledgment** This research was partially funded by an academic grant from Siemens Medical Solutions, Erlangen, Germany. We thank Siemens Medical Solutions for providing the sphere data.

### REFERENCES

- [1] Schmidt, G. P., Reiser, M. F., and Baur-Melnyk, A., "Whole-body imaging of the musculoskeletal system: the value of mr imaging.," *Skeletal Radiol* **36**, 1109–1119 (Dec 2007).
- [2] Lauenstein, T. C., Goehde, S. C., Herborn, C. U., Goyen, M., Oberhoff, C., Debatin, J. F., Ruehm, S. G., and Barkhausen, J., "Whole-Body MR Imaging: Evaluation of Patients for Metastases," *Radiology* **233**(1), 139–148 (2004).
- [3] Goyen, M., [*Real Whole Body MRI: Requirements, Indications, Perspectives*], McGraw-Hill (2007).

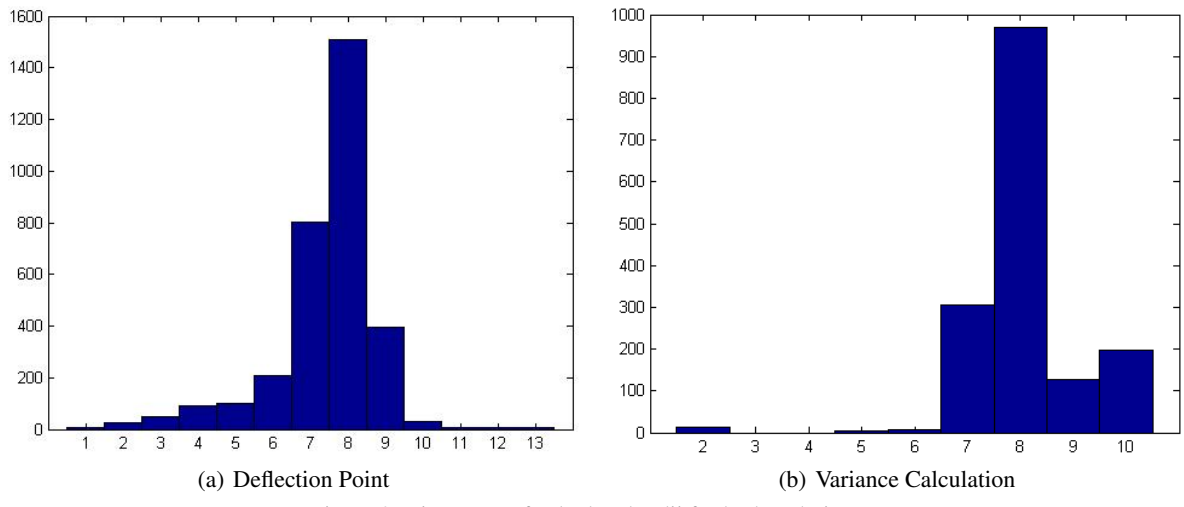


Figure 8. Histogram of calculated radii for both techniques.

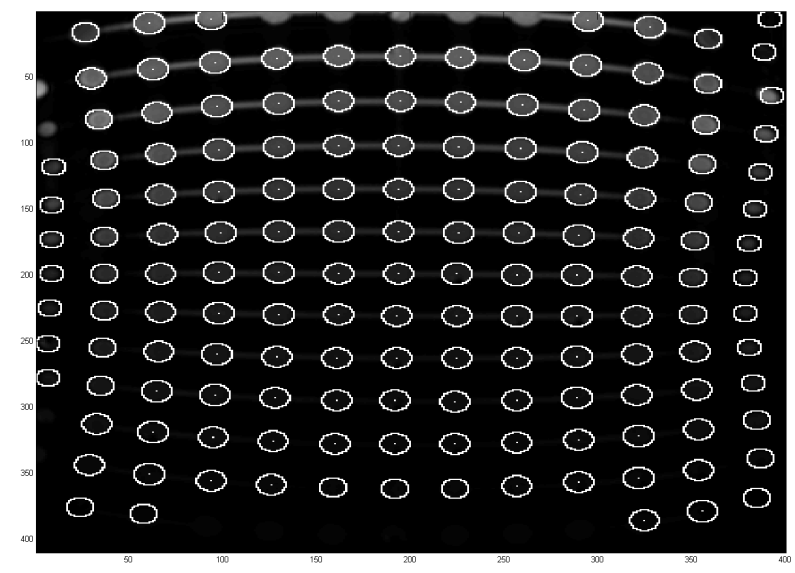


Figure 9. Final result of the extraction with augmented center points and spheres.

- [4] Wachinger, C., Glocker, B., Zeltner, J., Paragios, N., Komodakis, N., Hansen, M. S., and Navab, N., "Deformable Mosaicing for Whole-body MRI," in [*International Conference on Medical Image Computing and Computer-Assisted Intervention (MICCAI)*], (September 2008).
- [5] Chen, Z., Ma, C.-M., Paskalev, K., Li, J., Yang, J., Richardson, T., Palacio, L., Xu, X., and Chen, L., "Investigation of mr image distortion for radiotherapy treatment planning of prostate cancer.," *Phys Med Biol* **51**, 1393–1403 (Mar 2006).
- [6] Chang, H. and Fitzpatrick, J., "A technique for accurate magnetic resonance imaging in the presence of field inhomogeneities," *IEEE TMI* **11**(3), 319–329 (1992).
- [7] Kannengiesser, S., Wang, Y., and Haacke, E., "Geometric distortion correction in gradient-echo imaging by use of dynamic time warping," *Magnetic Resonance in Medicine* **42**(3), 585–590 (1999).
- [8] Reinsberg, S., Doran, S., Charles-Edwards, E., and Leach, M., "A complete distortion correction for MR images: II. Rectification of static-field inhomogeneities by similarity-based profile mapping," *Phys Med Biol* **50**(11), 2651–2661 (2005).
- [9] Doran, S., Charles-Edwards, L., Reinsberg, S., and Leach, M., "A complete distortion correction for MR images: I. Gradient warp correction," *Physics in Medicine and Biology* **50**(7), 1343–1361 (2005).
- [10] Ballard, D., "Generalizing the Hough transform to detect arbitrary shapes," *Pattern Recognition* **13**(2), 111–122 (1981).
- [11] Felsberg, M. and Sommer, G., "The monogenic signal," *IEEE Transactions on Signal Processing* **49**, 3136–3144 (December 2001).
- [12] Grau, V., Becher, H., and Noble, J. A., "Phase-based registration of multi-view real-time three-dimensional echocardiographic sequences," in [*MICCAI*], 612–619 (2006).
- [13] Grau, V., Becher, H., and Noble, J., "Registration of multiview real-time 3-d echocardiographic sequences," *Medical Imaging, IEEE Transactions on* **26**(9), 1154–1165 (Sept. 2007).